Biochimica et Biophysica Acta 1850 (2015) 393–400

Contents lists available at ScienceDirect

Biochimica et Biophysica Acta

journal homepage: www.elsevier.com/locate/bbagen

Chemical and thermal influence of the $[4Fe–4S]^{2+}$ cluster of A/G-specific adenine glycosylase from *Corynebacterium pseudotuberculosis*

Raphael J. Eberle [a], Monika A. Coronado [a], Icaro P. Caruso [a], Débora O. Lopes [b], Anderson Miyoshi [c], Vasco Azevedo [c], Raghuvir K. Arni [a,*]

[a] Multiuser Center for Biomolecular Innovation, Departament of Physics, Universidade Estadual Paulista (UNESP), São Jose do Rio Preto, SP 15054-000, Brazil
[b] Laboratory of Molecular Biology, Federal University of São João Del-Rei (CCO), Av. Sebastião Gonçalves Coelho, 400, Divinópolis, MG 35501-296, Brazil
[c] Laboratório de Genética Celular e Molecular, Instituto de Ciências Biológicas, Universidade Federal de Minas Gerais, Av. Antônio Carlos, 6627-Pampulha, CP 486, CEP 31, Belo Horizonte, MG 270-901, Brazil

ARTICLE INFO

Article history:
Received 18 August 2014
Received in revised form 28 October 2014
Accepted 14 November 2014
Available online 20 November 2014

Keywords:
C. pseudotuberculosis
MutY
$[4Fe–4S]^{2+}$ cluster
DNA repair
Spectroscopic method
Secondary and tertiary structure

ABSTRACT

The gram-positive bacteria *Corynebacterium pseudotuberculosis*, the causative agent of caseous lymphadenitis in livestock significantly reduces productivity and often causes death. The adenine/guanine-specific DNA glycosylase (MutY) prevents mutations in the DNA of the pathogen and a unique feature of the MutY protein family is the $[4Fe–4S]^{2+}$ cluster that interlinks two protein subdomains. MutY from *C. pseudotuberculosis* was expressed in *E. coli* and purified, the CD experiments indicate a high content of α-helices and random coiled secondary structure and a typical near-UV CD fingerprint for the $[4Fe–4S]^{2+}$ cluster. EDTA and copper sulfate possess a strong destabilizing effect on the $[4Fe–4S]^{2+}$ cluster. UV–vis and fluorescence spectroscopy results demonstrate that between pH 3.0 and 4.0 the integrity of the $[4Fe–4S]^{2+}$ cluster is destroyed. To investigate the thermal stability of the protein differential scanning calorimetry and fluorescence spectroscopy were used and the T_m was determined to be 45 °C. The analysis presented provides information concerning the protein stability under different physio-chemical conditions.

1. Introduction

Corynebacterium pseudotuberculosis (*C. pseudotuberculosis*) is a gram-positive bacterium which together with mycobacterium, nocardia and rhodococcus forms the 'CMNR group' of potential animal and human pathogens [1]. *C. pseudotuberculosis*, a facultative intracellular parasite is the causative agent of caseous lymphadenitis (CLA) in equids, sheep and goats (biovar ovis) and also to a lesser extent in horses and cattle (biovar and equus). Infection by *C. pseudotuberculosis* in sheep and goats leads to considerable economic loss due to significantly reduced yields in wool and milk production, weight loss, carcass condemnation and death due to the formation of abscesses in superficial and visceral lymph nodes and caseous necrosis of the lymphatic glands [2,3]. This pathogen is capable of survival and growth in macrophages thus evading detection by the host immune system [4,5]. Infections due to *C. pseudotuberculosis* are predominantly observed in sheep and goats and infections by this pathogen, although rare, have been reported to occur in humans [6–8]. In macrophages, *C. pseudotuberculosis* is exposed to an environment rich in reactive oxygen and nitrogen species (ROS and RNS, respectively) [9] in addition to those it endogenously generates during metabolism. These molecules interact with DNA ultimately causing different types of damage including the formation of modified bases, formation of abasic sites, and strand breaks, with cytotoxic or mutagenic effects on the cell [10,11]. Organisms have evolved various defense systems to protect their genomes from oxidative DNA damage; the base excision repair (BER) mechanism is the major repair pathway for the oxidized DNA bases and is initiated by DNA glycosylases. 7,8-dihydro-8-oxo-2′-deoxyguanosine (8-OxoG), one of the most stable oxidized purines, has the most deleterious effects because it can mispair with adenine during DNA replication [12,13]. The adenine/guanine-specific DNA glycosylase (MutY) [EC 3.2.2] plays an important role in the BER pathway and prevents DNA mutations resulting from the presence of the oxidatively damaged 8-OxoG. This guanosine derivate can mispair with 2′-deoxycytidine 5′-triphosphate or with 2′-deoxyadenosine triphosphate during DNA replication, forming C*8-oxoG and A*8-oxoG mispairs. If uncorrected, the A*8-OxoG mispairs can result in deleterious C:G to A:T transversions.

Abbreviations: CLA, caseous lymphadenitis; ROS, reactive oxygen species; RNS, reactive nitrogen species; MutY, adenine/guanine-specific DNA glycosylase; IPTG, isopropyl-β-D-thiogalactopyranosid; CD, circular dichroism spectroscopy; DSC, differential scanning calorimetry; UV–vis, ultraviolet–visible spectroscopy; Trp, tryptophane; REES, red edge excitation shift

* Corresponding author at: Centro Multiusuário de Inovação Biomolecular, Departamento de Física, Universidade Estadual Paulista (UNESP), Rua Cristóvão Colombo 2265, São Jose do Rio Preto, SP 15054-000, Brazil. Tel.: +55 17 32212460; fax: +55 17 32212247.
E-mail address: arni@sjrp.unesp.br (R.K. Arni).

http://dx.doi.org/10.1016/j.bbagen.2014.11.014
0304-4165/

MutY, with its DNA glycosylase activity, excises adenine paired with guanine or 8-OxoG.

A unique feature of the MutY protein family is that the enzymes contain a $[4Fe–4S]^{2+}$ cluster [14–17]. This cluster forms a cuboidal structure where the iron and sulfide ions are arranged in two overlapping tetrahedrons. The four iron atoms of the cluster are coordinated via a conserved and unique spacing of cysteine thiolates, Cys-X6-Cys-X2-Cys-X5-Cys. The $[4Fe–4S]^{2+}$ cluster connects two subdomains of the MutY proteins, a 4α-helical domain with a 6α-helical bundle, containing a helix–hairpin–helix motif [15]. In the present study, we investigate the *C. pseudotuberculosis* MutY by employing a host of spectroscopic techniques (UV, vis, fluorescence, circular dichroism (CD)) and differential scanning calorimetry (DSC), to probe the role of the $[4Fe–4S]^{2+}$ cluster in the stability of the protein under different chemical and thermal conditions.

2. Material and methods

2.1. In silico analysis

Sequence alignments of different MutY proteins were performed with the ClustalW2 online Tool [18] and the secondary structure of the protein was predicted with the PSIPRED server [19,20].

The atomic coordinates of MutY from *E. coli* (PDB: 1KG7) were used as a template in comparative modeling by the satisfaction of spatial restraints as implemented in the program Modeller 9v13 [21] to model the structure of MutY (Uniprot:D9Q4I3). Due to the poor correlation, the N-terminal amino acids 1–10 and the C-terminal amino acids 222–295 of *C. pseudotuberculosis* MutY were deleted.

2.2. Cloning

The MutY gene was amplified from genomic DNA of *C. pseudotuberculosis* (1002) through PCR using 5′-GGATCCGTGA CATTGCACTCAGGTA-3′ and 5′-CTCGAGCCTGGGCAGATGGAAAAAA-3′ oligonucleotides which have restriction sites for *Bam*HI and *Xho*I enzymes, respectively. The fragment was purified from an agarose gel and cloned into the pGEM-T Easy propagation vector (Promega) to yield the pGEM-CpmutY construct. The construct was subsequently digested with *Bam*HI and *Xho*I enzymes and the fragment released was subcloned into the pET-21a expression vector (Novagen), yielding the pET-CpmutY construct. The clonal sequence was confirmed by DNA sequencing analysis, performed on a MegaBACE 1000 automated sequencer (GE Healthcare) at the Nucleus for Genome Analysis and Gene Expression (NAGE) of the Biological Sciences Institute, at the Universidade Federal de Minas Gerais.

2.3. Expression and purification

E. coli BL21 (DE3) pLysS (Invitrogen, USA) cells were transformed with the MutY pET-21a construct. Single colonies were picked and grown overnight in Luria–Bertani medium supplemented with 0.5 M sorbitol and 1 mM betaine. The bacterial culture was diluted to 1:100 and grown at 37 °C until the OD_{600} reached 0.5. Expression was initiated with 0.5 mM isopropyl-β-D-thiogalactopyranoside (IPTG) and the cells were grown for 20 h at 18 °C before harvesting. The cell pellet was suspended in buffer A (50 mM Tris buffer pH 7.5, 500 mM NaCl, 10% glycerol, 20 mM imidazole), sonicated and centrifuged at 50.000 ×*g* for 1 h at 4 °C. The soluble fraction of the lysate was applied onto a Ni–NTA column previously incubated in buffer A. The bound sample was washed extensively in buffer A with an increasing imidazole gradient. MutY eluted at 250 mM imidazole, the purity of the sample was assessed on SDS–PAGE [22]. The elution fraction was injected onto a Superdex 75 10/300 GL (GE Healthcare) size exclusion column pre-equilibrated with buffer B (20 mM Tris pH 8.0, 150 mM NaCl). The purity of the sample was assessed by SDS–PAGE gels [22].

2.4. Ultraviolet–visible spectroscopy (UV–vis)

For the UV–vis spectroscopy measurements a Cary 3Bio UV-visible spectrophotometer (Varian, USA) was used. The protein concentration was 60 μM in 50 mM K_2HPO_4/KH_2PO_4 pH 8.0 and 150 mM NaCl. The measured wavelength was between 300 and 600 nm. Cuvettes of 1.0 cm path length were used for the experiments.

The pH influence of the protein was investigated in 50 mM K_2HPO_4/KH_2PO_4 pH 8.0 and 150 mM NaCl. The protein concentration was 6 μM. The cuvette had a path length of 5 cm. The protein solution within the cuvette was stepwise titrated with conc. HCl to pH 3.0 and each 30 min a measurement was performed.

2.5. Circular dichroism spectroscopy (CD)

CD measurements were conducted in a Jasco J-701 spectropolarimeter (Jasco, USA). Far-UV spectra were measured from 200 to 260 nm range and near-UV spectra from 250 to 700 nm range. Protein concentration used for the far-UV CD measurements was 10 μM and for the near-UV measurements 116 μM. Cells of 1.0 cm path length were used for the measurements of the far- and near-UV spectra, respectively. 15 repeat scans were obtained for each sample and five scans were conducted to establish the respective baseline. The averaged baseline spectrum was subtracted from the averaged sample spectrum. The protein was dissolved in 20 mM K_2HPO_4/KH_2PO_4 pH 8.0 and 50 mM NaCl. For investigation of EDTA influence a 0.5 M EDTA stock solution was used and dissolved with the protein solution and the corresponding buffer to an end-concentration of 1 mM EDTA. The protein was incubated with the EDTA at 4 °C for 10 min, 1 h, 24 h and 48 h. As a control, the pH values of the protein solutions were determined before and after each measurement. The influence of different ions was determined for cobalt chloride, cadmium chloride, zinc sulfate, lithium sulfate, and copper sulfate. The ion stock-solutions had a concentration of 100 mM and were dissolved with the protein solution and the corresponding buffer to obtain a final concentration of 1 mM. The influence of the pH on the secondary structure of MutY was checked using KCl–HCl (pH 0.5–1.5), Gly–HCl (pH 2.0–3.5), sodium acetate (pH 4.0–5.5), sodium phosphate (pH 6.0–8.0) and Tris–HCl (pH 8.5–10.0). Concentrations of all buffers were 50 mM. A stock solution of the protein was added to the appropriate buffer. The mixture was measured after 1 h at 4 °C. Results are expressed as molar ellipticity [θ] (deg cm^2 $dmol^{-1}$), calculated from the following formula $[\theta]\lambda = \theta / [c] * l * 10 * n$, where θ is the measured ellipticity in degrees at wavelength λ, c is the protein concentration in mg ml^{-1}, l is the light path length in centimeters and n is the number of amino acids. For the analysis of the CD data the program CDPro [23] was used.

2.6. Differential scanning calorimetry (DSC)

The DSC experiments were performed on N-DSC III (TA Instruments, USA) in the range of 20–90 °C with a scan rate of 1 °C/min. For the DSC experiments the protein concentration was 20 μM and the buffer for the measurements contained 50 mM K_2HPO_4/KH_2PO_4 pH 8.0 and 150 mM NaCl. Both the calorimeter cells were loaded with the buffer solution, equilibrated at T = 20 °C for 10 min, and scanned as previously mentioned. The buffer scans were repeated till the baseline was reproducible. After, the sample cell was rinsed and loaded with MutY and then scanned in the same range. The excess heat capacity versus temperature scan for the protein transition was obtained by subtracting the corresponding scan of buffer versus buffer from that of the protein solutions versus buffer.

2.7. Fluorescence spectroscopy

The intrinsic Trp fluorescence was measured with an ISS PC1 steady-state spectrofluorimeter (Champaign, IL, USA) equipped with a quartz

cell of 1 cm path length and Neslab RTE-221 thermostat bath. Both excitation and emission bandwidths were set at 8.0 nm. The excitation wavelength at 295 nm was chosen since it provides no excitation of tyrosine residues. The emission spectrum was collected in the range of 305–500 nm with the increment of 1 nm. Each point in the emission spectrum is the average of 10 accumulations. The protein solution had a concentration of 8 μM and the measuring volume was 2 ml. The buffer for the experiment contained 50 mM K_2HPO_4/KH_2PO_4 pH 8.0 and 150 mM NaCl. During the investigation of the pH of MutY, the protein solution within the cuvette was stepwise titrated with conc. HCl to pH 3.0 and each 30 min a measurement was conducted. The measurement of thermal unfolding MutY was performed in the range of 20–85 °C with increments of 5 °C. The native protein fraction (f_N) was calculated according to the following equation:

$$f_N = (F - F_U)/(F_N - F_U)$$

where F, F_N and F_U are the steady-state fluorescence intensities of Trp at each temperature investigated, at the first (native protein) and the last (unfolded protein) temperature, respectively. The unfolded protein fraction can be calculated as follows: $f_U = 1 - f_N$. The temperature at which $f_N = f_U$ is called melting temperature or transition midpoint (T_m). Using the two-state transition model for the unfolding protein and calculating equilibrium constant between the native (folding) and denatured (unfolding) states of the protein, $K_{eq} = f_U / f_N$, the enthalpy (ΔH_U) and entropy changes (ΔS_U) of the unfolding reaction using van't Hoff plot and $\Delta S_U = \Delta H_U / T_m$ can be determined, respectively.

3. Results and discussion

3.1. Sequence analysis and molecular modeling

A blast search of the *C. pseudotuberculosis* MutY indicated a highly conserved protein sequence within the genus *Corynebacterium*, with a sequence identity of up to 93% (*C. ulcerans*) (Fig. 1). The MutY sequence alignment across the bacterial genera confirms the conservation of motifs which are important for protein specific functions and structure, such as the Fe–S cluster building FCL motif and the helix–hairpin–helix DNA-binding motif [16]. The Fe–S cluster-containing protein MutY from *C. pseudotuberculosis* possesses a highly conserved FCL motif, (Cys-(Xaa) 6-Cys-(Xaa)2-Cys-(Xaa)5-Cys) [14], formed by Cys 197, Cys 203, Cys 206 and Cys 212 (Fig. 1). This FCL motif is required for the formation of the Fe–S cluster which, in the MutY family is the $[4Fe–4S]^{2+}$ cluster interlinking two protein subdomains [15,14,24].

Although the sequence alignment between *C. pseudotuberculosis* MutY with the structure of *E.coli* MutY (PDB: 1KG7) is only around 31%, the molecular model of *C. pseudotuberculosis* MutY shares a high structural homology with the *E.coli* MutY (Figs. 2A and Fig. B, C Supplementary material).

Even though the sequence identity is low, the *C. pseudotuberculosis* and *E. coli* proteins possess a highly conserved fold. The MutY model shows the typical helix–hairpin–helix (HhH) motif of the DNA repair enzyme superfamily, with an all-α helical fold comprised of two domains: a six-α helix barrel domain and a four-α helix domain that is structurally coordinated by the $[4Fe–4S]^{2+}$ cluster. These domains possess an electrostatically positive surface that binds DNA. This architecture is a characteristic of the canonical Endo III HhH glycosylase fold that is encountered in the large superfamily of DNA repair glycosylases [26]. Interestingly, the presence of a $[4Fe–4S]^{2+}$ cluster in

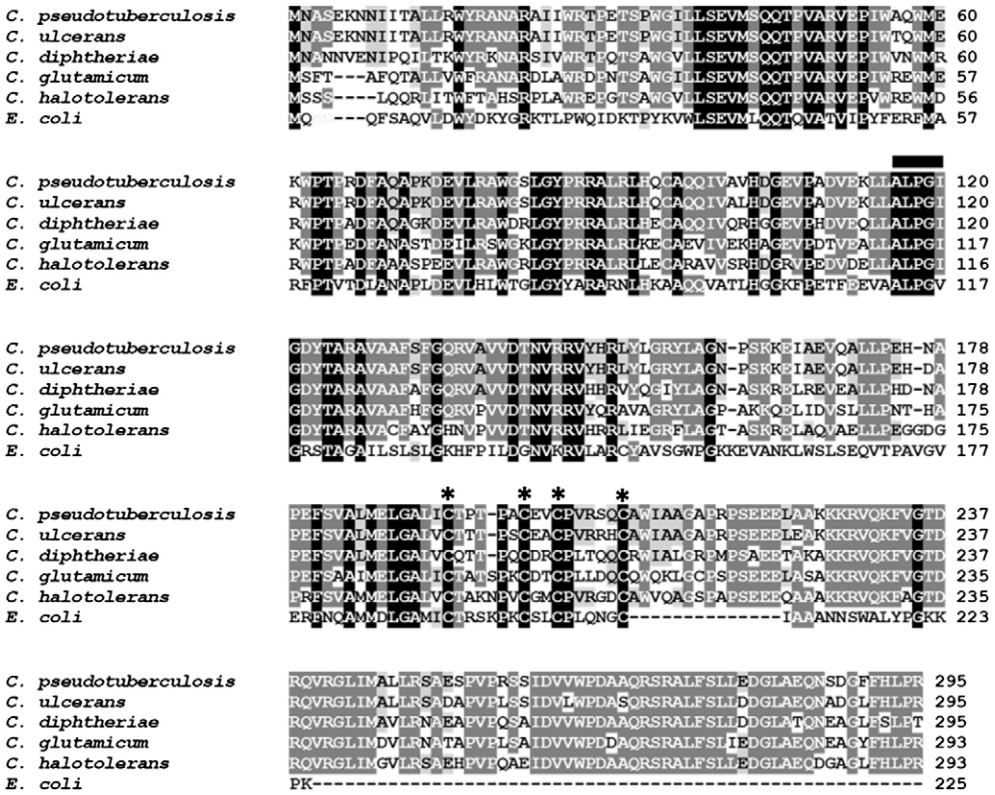

Fig. 1. Sequence alignment of MutY from *C. pseudotuberculosis* (ADK29561.1), *C. ulcerans* (BAM28184.1), *C. diphteriae* (AEX81840.1), *C. glutamicum* (AGT06387.1), *C. halotolerans* (AGF73423.1) *and E. coli* (AAA72957.1; PDB: 1KG7). The asterisk highlights the FCL motif, the black bar indicates the helix–hairpin–helix (HhH) DNA-binding motif which interact with the phosphate backbone of the substrate [25].

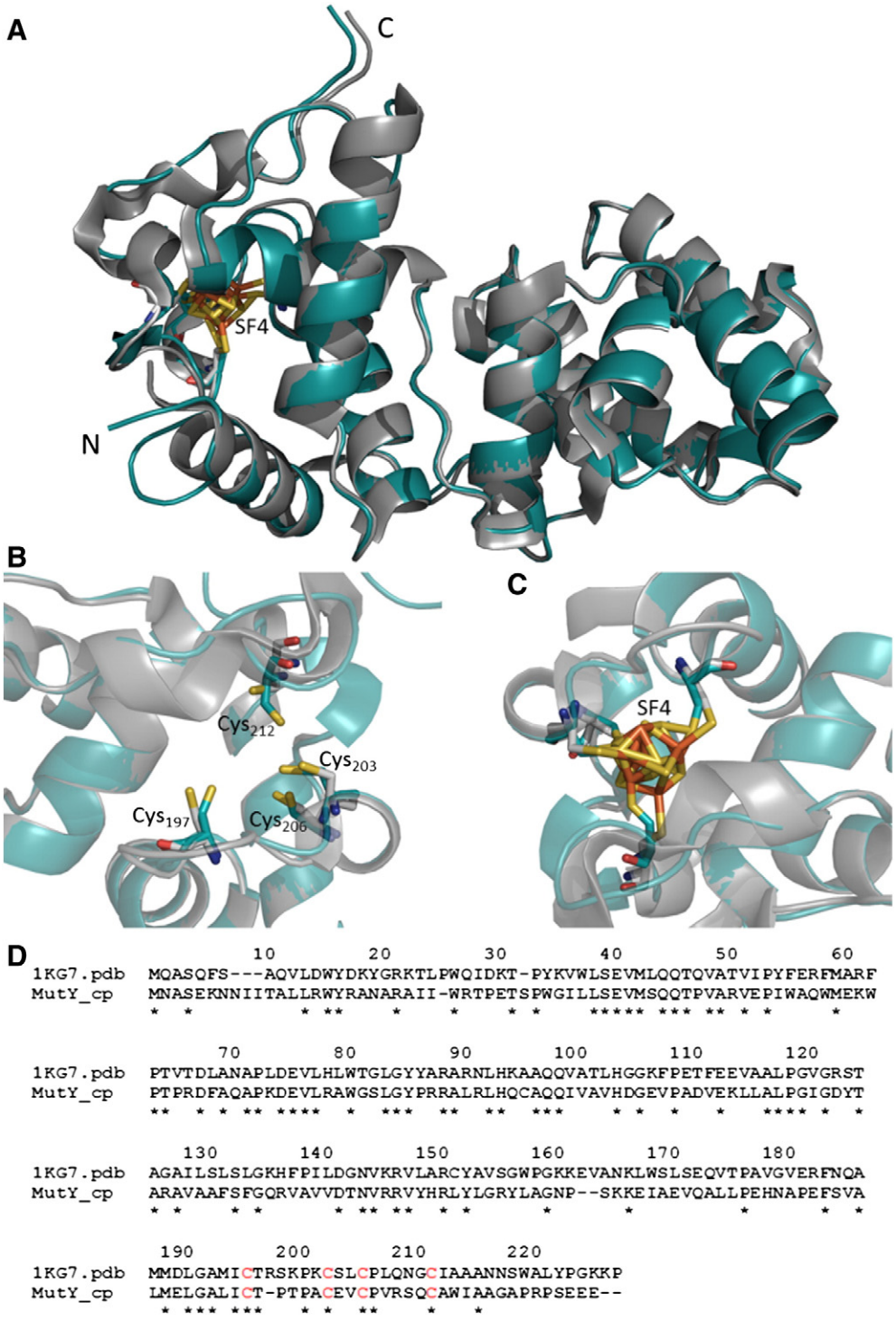

Fig. 2. Homology model of *C. pseudotuberculosis* MutY. A: superposition of the *C. pseudotuberculosis* MutY model in turquoise and the *E. coli* MutY structure (PDB: 1KG7) in gray, the Fe–S (SF4) cluster is highlighted. B: superposition of the four cysteine residues of the FCL-motif. C: superposition of the FCL-motif with coordinated SF4 cluster. D: sequence alignment of *C. pseudotuberculosis* MutY and *E. coli* MutY, the conserved cysteine residues of the FCL-motif colored in red.

several DNA repair enzymes, like MutY, is unusual since iron–sulfur clusters are commonly encountered in proteins involved in electron-transfer reactions [27].

3.2. Expression and purification

MutY from *C. pseudotuberculosis* was cloned with a 6x-histidine affinity tag and expressed in *E. coli* BL21 (DE3) pLysS cells. The highest protein expression levels were obtained by induction overnight with 0.5 mM IPTG at 20 °C. The protein consists of 301 amino acids with a molecular weight of 33.703 Da as calculated from its amino-acid sequence. The purified protein was present as a single band with a mass of 35 kDa on SDS–PAGE gels (Fig. A (Supplementary material)), which is in agreement with the full length protein in fusion with the N-terminal 6x His tag. The fraction containing the protein was brown–yellow in color indicating the presence of Fe–S clusters, even after

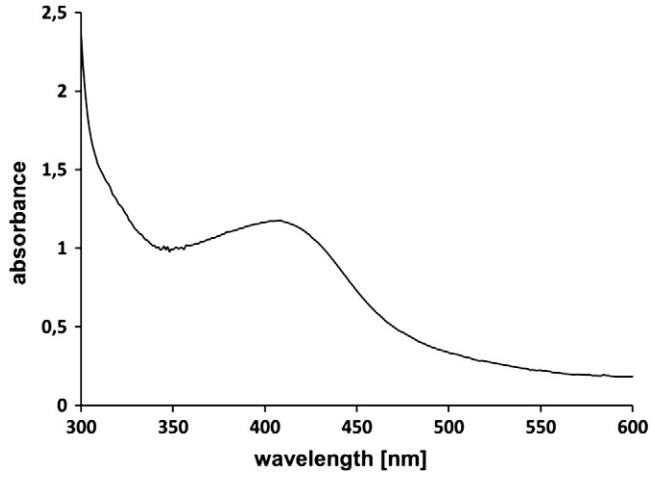

Fig. 3. Characterization of MutY. A: UV–vis spectra of MutY between 300 and 600 nm, with the characteristic absorbance for $[4Fe–4S]^{2+}$ proteins around 420 nm.

purification [28]. Dynamic light scattering experiments indicated a dimeric state in solution for the recombinant protein (data not shown), as observed for one homologous MutY protein in the crystal structure [15].

3.3. Determination of the Fe–S cluster in MutY by UV–vis scanning

The UV–vis spectra of the recombinant produced *C. pseudotuberculosis* MutY presented in Fig. 3 possess a characteristic broad peak between 350 and 450 nm centered around 410 nm, which is attributed to the thiolate to iron charge transfer transitions from cysteines ligating the $[4Fe–4S]^{2+}$ cluster [24,29].

3.4. Investigation of the secondary and tertiary structure of MutY using CD spectroscopy

The far-UV and near-UV spectra of native *C. pseudotuberculosis* MutY are presented in Fig. 4.

The far-UV CD spectrum of MutY is characterized by the presence of two relative minima at 208 and 224 nm suggesting the presence of large α-helical content in its secondary structure. The near-UV CD spectrum of MutY revealed two characteristic maxima at 330 and 420 nm as described earlier for $[4Fe–4S]^{2+}$ cluster containing proteins [30,31]. A secondary structure prediction for *C. pseudotuberculosis* MutY with the online tool PSIPRED [19,20] demonstrated that the dominant secondary structure elements are α-helices and coiled regions. The predicted α-helical amount is 51%, coiled regions 47% and β-sheet 2%.

The results of the secondary structure prediction of MutY correspond to the results of the far-UV CD measurements that show a high α-helical and random coiled content in the secondary structure of MutY. The analysis of the CD results with the program CDpro [23] showed for MutY 60% α-helices, 34% coiled regions and 7% β-sheet. Both methods indicated a high α-helical and random coiled content in the secondary of the protein, these results are in agreement with the existing 3D structures of the MutY proteins that contain a high amount α-helices (>60%) in the secondary structure [14,24].

3.5. Investigation of chemical influence on the $[4Fe–4S]^{2+}$ cluster and secondary and tertiary structure of MutY

Protein conformational changes and the influence on the Fe–S cluster induced by altering the net charge through pH titrations, the influence of EDTA and different ions were monitored using the far-UV and the near-UV CD spectroscopy, UV–vis spectroscopy and fluorescence spectroscopy.

A weak EDTA effect on the near-UV CD spectra was observed after incubation for 24 h, after incubation for 48 h, the iron–sulfur cluster was completely destabilized. In contrast, a reduction of 60% in the MutY far-UV CD spectra after incubation for 24 h was observed (Fig. 5A and B). During unfolding processes, the Fe–S cluster protein ferredoxin, forms transient states in which the polypeptide suffers conformational rearrangements to maintain contacts with the iron–sulfur clusters [32,33]. This attribute of a Fe–S containing protein could explain the observed EDTA effect of MutY where the secondary structure dissolved almost completely after 24 h and the polypeptide chain reorganizes in a conformation that maintains contact with the Fe–S cluster, the observed tertiary structural changes are slow compared to the secondary structural changes of the protein.

Cobalt chloride, zinc sulfate, copper sulfate and cadmium chloride ions showed a strong effect on the secondary structure of MutY (Fig. 5C). The strongest effects were observed for 1 mM copper sulfate that completely destroyed the iron–sulfur cluster in the appropriate near-UV CD spectrum (Fig. 5 D) and the secondary structure in the far-UV regions. It was shown before, that cadmium (II), mercury (II), silver (I), zinc (II) and copper (I) had a destructive effect on Fe–S cluster containing proteins [34].

Copper ions showed the strongest effect on the MutY protein, followed by cadmium, cobalt and zinc ions. Heavy metal cations may cause toxicity by tight association with sulfhydryl groups of proteins [35]. The ions displace the iron in the cluster and interact with the sulfur as observed before.

In contrast, lithium sulfate shows no strong denaturing effect on the protein and a decrease of the α-helical content and an increase in the random coiled fraction were observed (Fig. 5C). Inclusion of lithium sulfate resulted in a stepwise decrease of the intrinsic Trp fluorescence at 295 nm (data not shown). This effect of lithium on proteins has been

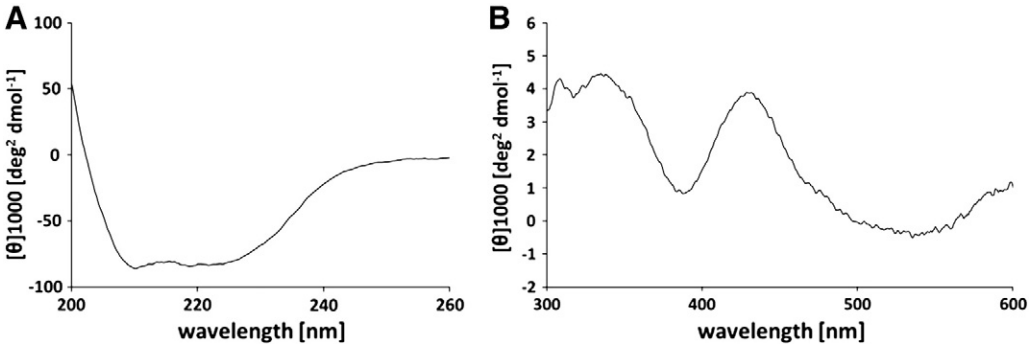

Fig. 4. CD spectroscopic measurements of *C. pseudotuberculosis* MutY. A: far-UV CD spectrum of MutY from 200 to 260 nm wavelength. The far-UV CD spectrum shows two minima at 208 and 224 nm and suggests the presence of a high α-helical content in the secondary structure of MutY. B: near-UV CD spectrum and tertiary structure "fingerprint" of MutY between 300 and 600 nm.

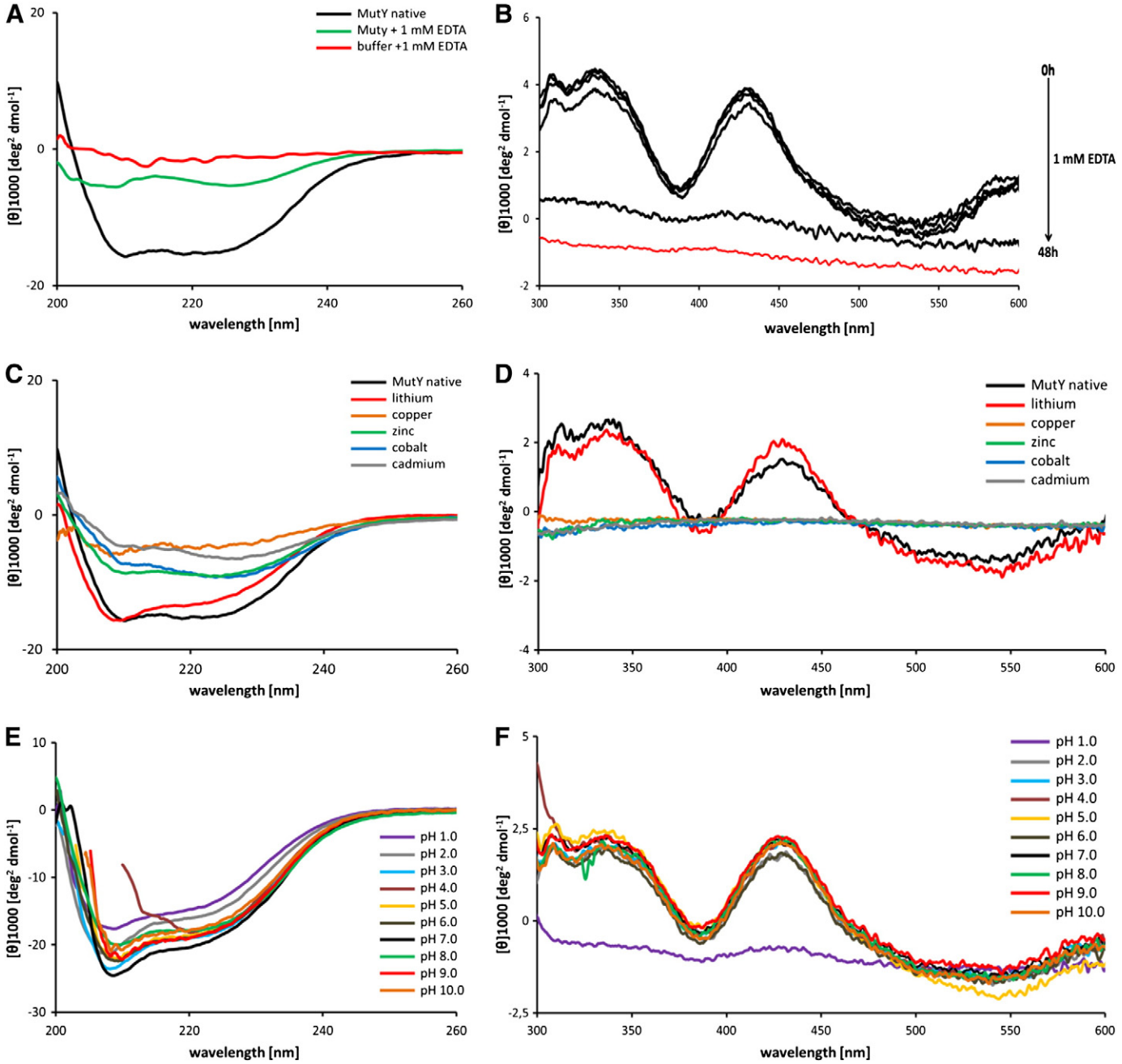

Fig. 5. CD spectroscopic measurements of MutY. A: Far-UV CD spectra of MutY under the influence of 1 mM EDTA incubated for 48 h (green line) compared with native MutY (black line) and the buffer + 1 mM EDTA (red line). B: Near-UV CD spectra of MutY under the influence of 1 mM EDTA were incubated for 10 min, 1 h, 24 h and 48 h and the buffer + 1 mM EDTA (red line). C: Far-UV CD spectra of MutY under the influence of 1 mM cobalt chloride, cadmium chloride, zinc sulfate, lithium sulfate, and copper sulfate. D: Near-UV CD spectra of MutY under the influence of 1 mM ions as described earlier. E: Far-UV CD spectra of MutY under the influence of pH 1.0, 2.0, 3.0, 4.0, 5.0, 6.0, 7.0, 8.0, 9.0 and 10.0. F: Near-UV CD spectra of MutY under the influence of pH 1.0 to 10.0.

described earlier [36–38] and is based on the direct interaction with carboxylate groups present on the protein surface [38].

MutY possesses a high stability in the pH 2.0 to 10.0 range as evidenced by the far- and near-UV CD spectra (Fig. 5E and F). Interestingly, at pH 4.0 the secondary structure content changes from α-helical to β-sheet, in which the near-UV CD spectrum seems unaffected. UV–vis and intrinsic Trp fluorescence spectroscopy experiments conducted at pH 3.0 on the MutY Fe–S cluster indicated that after 4 h the $[4Fe–4S]^{2+}$ cluster was completely destroyed (Fig. 6).

Intrinsic tryptophan (Trp) fluorescence and red edge excitation shift (REES) were used to evaluate the Trp conformational freedom and flexibility. MutY has nine Trp, in the native state the emission is partially quenched by the metal center [38] and the surrounding amino acids [37, 38]. The maximum Trp emission in MutY at pH 8.0 was centered at 330 nm, at pH 3.0 this emission band shifted to 340 nm. This indicates a partially disordered conformation in the protein due to the loss of secondary and tertiary structure, permitting water penetration near some of the tryptophan residues, which results in a red shift in the emission spectra maximum [37]. The far-UV CD spectra of the protein at pH 3.0 indicated an increased amount of unfolded regions (Fig. 5E) however; α-helical regions are still present. In addition MutY in pH 3.0 exhibits an increase of 40% in the Trp fluorescence intensity relative to the protein at pH 8.0. This result indicates the possible release of intramolecular quenching of tryptophan fluorescence through the Fe–S cluster.

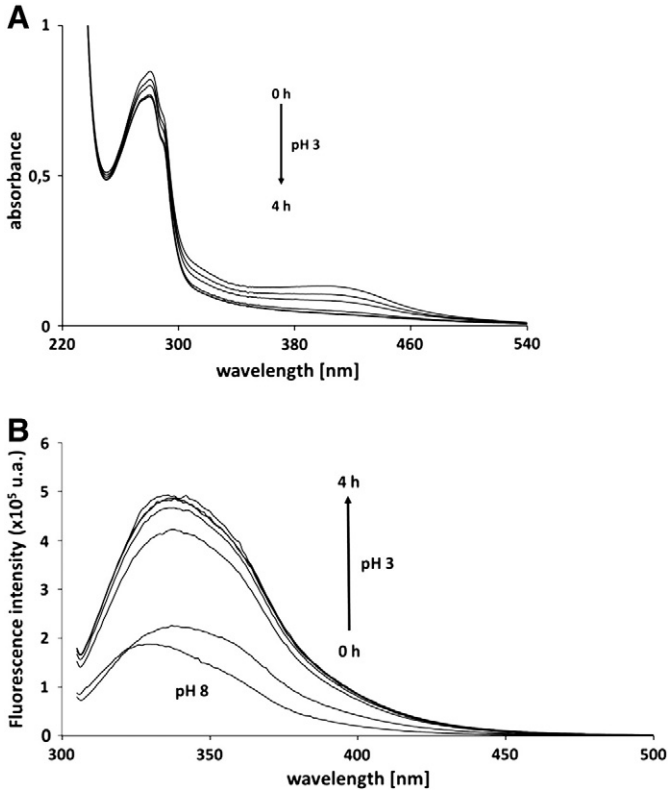

Fig. 6. Influence of pH 3.0 of the MutY Fe–S cluster. A: UV–vis spectroscopy of MutY under the influence of pH 3.0 during 4 h incubation. The Fe–S cluster disassembles completely but very slowly over a time period of 4 h. B: Fluorescence spectroscopy of Trp at 295 nm in MutY. In pH 3.0 is a red edge excitation shift (REES) of Trp visible, and the tryptophan was moved from a hydrophilic to a hydrophobic environment.

3.6. Investigation of thermal influence on the [4Fe–4S]$^{2+}$ cluster and secondary and tertiary structure of MutY

Temperature is a standard mode of protein denaturation method, and structural changes can induce and hence provide ample information. Thermal experiments were monitored by intrinsic Trp fluorescence spectroscopy and DSC. The intrinsic Trp fluorescence decreases by increasing the temperature from 20 °C to 85 °C (Fig. 7A). A shift in the Trp emission as described at pH 3.0 influence over time (Fig. 6B) was not observable. The fraction of the native protein (f_N) decreases during increasing of the temperature and the fraction of the unfolded protein (f_U) increases during the same process. The intersection of both curves shows the transition midpoint (T_m) of MutY at 45 °C (Fig. 7B). The thermal unfolding reaction of MutY is irreversible and the protein was degraded after the experiments. Based on this experiment and using van't Hoff plot the values of ΔH_U and ΔS_U were 96 kJ/mol and 302 J/mol.K (Fig. 7C), respectively.

Additionally, DSC was used to observe the MutY thermal transition. The thermogram of MutY is dominated by a strong exothermic reaction centered at 45 °C that are likely arising from chemical reactions involving Fe–S compounds released by the protein upon thermal unfolding [39]. The transition midpoint of *C. pseudotuberculosis* MutY (45 °C) is similar to the T_m of the *E. coli* MutY with 46 °C [16].

4. Conclusions

DNA repair mechanisms in *C. pseudotuberculosis* remain poorly understood and research in this area can contribute to narrow the search for molecular targets against lymphadenitis. In silico analyses of DNA repair pathways of 15 *Corynebacterium* species, including *C. pseudotuberculosis* demonstrated that genes involved in oxidative damage repair, such as fpg/mutM (formamidopyrimidine-DNA glycosylase), nth/mutY (endonuclease III), nei/endoVIII (endonuclease VIII), and xht/exoIII (exonuclease III), are highly conserved, being

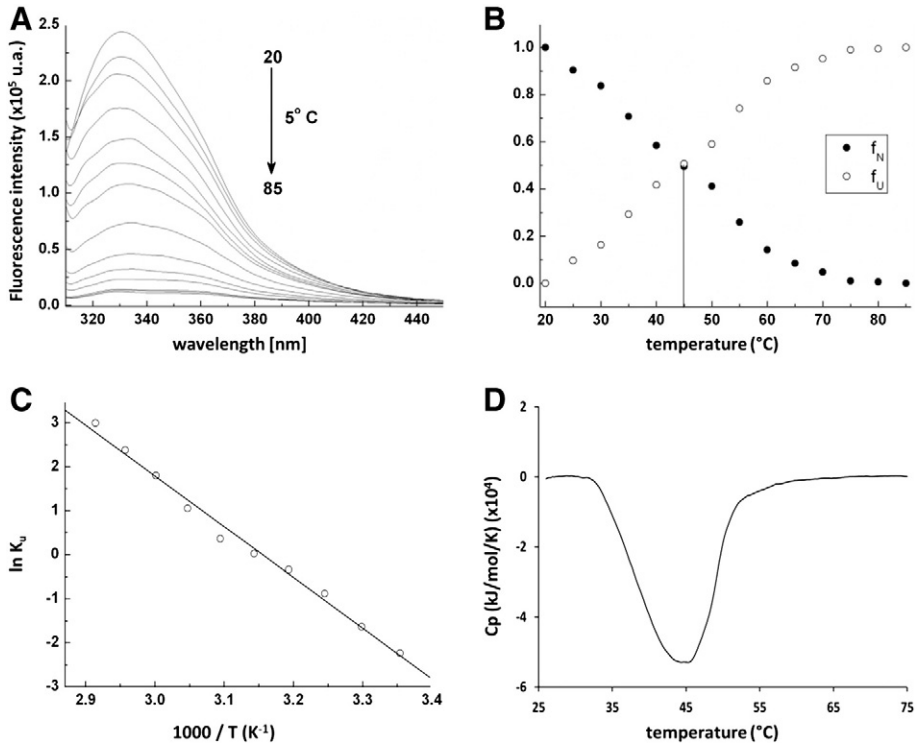

Fig. 7. Thermal investigation of MutY by intrinsic Trp fluorescence spectroscopy and DSC. A: Intrinsic Trp fluorescence at 295 nm at increasing temperature (20–85 °C) a decrease in the Trp fluorescence is observed and indicates the denaturation of the protein. B: Plot of the native protein fraction (f_N) and the unfolding protein fraction (f_U). With increasing temperature f_N decrease and f_U increase, on the intersection of both curves the melting temperature (T_m) of 45 °C was determined. C: van't Hoff plot of the MutY thermal denaturation. D: DSC thermogram of MutY, the thermogram shows a strong exothermic reaction at around 45 °C.

present in all investigated species. This suggests that repair of oxidative lesions is essential to ensure genomic stability and survival of these organisms [40].

The Fe–S cluster containing DNA repairing protein MutY from *C. pseudotuberculosis* was overexpressed and purified. The presence of the Fe–S cluster was demonstrated by UV–vis experiments and CD spectroscopy. These experiments indicated high content of α-helices and random coiled structures. These results are in agreement with secondary structure predictions and the available 3D structures of MutY proteins. Except for lithium, EDTA and other ions have a strong effect on the protein and the Fe–S cluster stability. Especially between pH 3.0 and pH 4.0 the protein undergoes a slow cluster disassembling effect suggesting large structural rearrangements. Thermal unfolding studies by two independent methods indicated a T_m of 45 °C. The chemical and the thermal influence on the binding behavior of MutY to DNA or related molecules will be very interesting to investigate in future research.

Acknowledgments

This research was supported by grants from the CNPq (Science without Frontiers), FAPESP, CAPES and FAPEMIG.

Appendix A. Supplementary data

Supplementary data to this article can be found online at http://dx.doi.org/10.1016/j.bbagen.2014.11.014.

References

[1] T.M. Embley, E. Stackebrandt, The molecular phylogency and systematics of the actinomycetes, Annu. Rev. Microbiol. 48 (1994) 257–289.
[2] J.L. Ayers, Caseous lymphadenitis in goats and sheep: a review of diagnosis, pathogenesis, and immunity, J. Am. Vet. Med. Assoc. 171 (1977) 1251–1254.
[3] L.H. Williamson, Caseous lymphadenitis in small ruminants, Vet. Clin. North Am. Food Anim. Pract. 17 (2001) 359–371.
[4] F.A. Dorella, L.G. Pacheco, S.C. Oliveira, A. Miyoshi, V. Azevedo, *Corynebacterium pseudotuberculosis*: microbiology, biochemical properties, pathogenesis and molecular studies of virulence, Vet. Res. 37 (2006) 201–218.
[5] S. McKean, J. Davies, R. Moore, Identification of macrophage induced genes of *Corynebacterium pseudotuberculosis* by differential fluorescence induction, Microbes Infect. 7 (2005) 1352–1363.
[6] T. Bregenzer, R. Frei, H. Ohnacker, W. Zimmerli, *Corynebacterium pseudotuberculosis* infection in a butcher, Clin. Microbiol. Infect. 3 (1997) 696–698.
[7] M.M. Peel, G.G. Palmer, A.M. Stacpoole, T.G. Kerr, Human lymphadenitis due to *Corynebacterium pseudotuberculosis*: report of ten cases from Australia and review, Clin. Infect. Dis. 24 (1997) 185–191.
[8] G. Funke, A. von Graevenitz, J.E. Clarridge, K.A. Bernard, Clinical microbiology of coryneform bacteria, Clin. Microbiol. Rev. 10 (1997) 125–159.
[9] C. Nathan, M.U. Shiloh, Reactive oxygen and nitrogen intermediates in the relationship between mammalian hosts and microbial pathogens, Proc. Natl. Acad. Sci. U. S. A. 97 (2000) 8841–8848.
[10] D.E. Barnes, T. Lindahl, Repair and genetic consequences of endogenous DNA base damage in mammalian cells, Annu. Rev. Genet. 38 (2004) 445–476.
[11] M. Dizdaroglu, P. Jaruga, Mechanisms of free radical-induced damage to DNA, Free Radic. Res. 46 (2012) 382–419.
[12] M.L. Michaels, J.H. Miller, The GO system protects organisms from the mutagenic effect of the spontaneous lesion 8-hydroxyguanine (7,8-dihydro-8-oxoguanine), J. Bacteriol. 174 (1992) 6321–6325.
[13] J. Tchou, A.P. Grollman, Repair of DNA containing the oxidatively-damaged base 8-hydroxyguanine, Mutat. Res. 299 (1993) 277–287.
[14] R.C. Manuel, K. Hitomi, A.S. Arvai, P.G. House, A.J. Kurtz, M.L. Dodson, A.K. McCullough, J.A. Tainer, R.S. Lloyd, Reaction intermediates in the catalytic mechanism of *E. coli* MutY DNA glycosylase, J. Biol. Chem. 379 (2004) 46930–46939.
[15] Y. Guan, R.C. Manuel, A.S. Arvai, S.S. Parikh, C.D. Mol, J.H. Miller, R.S. Lloyd, J.A. Tainer, MutY catalytic core, mutant and bound adenine structures define specificity for DNA repair enzyme superfamily, Nat. Struct. Mol. Biol. 5 (1998) 1058–1064.
[16] S.L. Porello, M.J. Cannon, S.S. David, A substrate recognition role for the $[4Fe–4S]^{2+}$ cluster of the DNA repair glycosylase MutY, Biochemistry 37 (1998) 6465–6475.
[17] R.P. Cunningham, H. Asahara, J.F. Bank, C.P. Scholes, J.C. Salerno, K. Surerus, E. Munck, J. McCracken, J. Peisach, M.H. Emptage, Endonuclease III is an iron–sulfur protein, Biochemistry 28 (1989) 4450–4455.
[18] M.A. Larkin, G. Blackshields, N.P. Brown, R. Chenna, P.A. McGettigan, H. McWilliam, F. Valentin, I.M. Wallace, A. Wilm, R. Lopez, J.D. Thompson, T.J. Gibson, D.G. Higgins, Clustal W and Clustal X version 2.0, Bioinformatics 23 (2007) 2947–2948.
[19] D.T. Jones, Protein secondary structure prediction based on position-specific scoring matrices, J. Mol. Biol. 292 (1999) 195–202.
[20] D.W.A. Buchan, F. Minneci, T.C.O. Nugent, K. Bryson, D.T. Jones, Scalable web services for the PSIPRED protein analysis workbench, Nucleic Acids Res. 41 (2013) 340–348.
[21] N. Eswar, M.A. Marti-Renom, B. Webb, M.S. Madhusudhan, D. Eramian, M. Shen, U. Pieper, A. Sali, Comparative protein structure modeling with modeller, Curr. Protoc. Bioinformatics 15 (2007) 1–30.
[22] U.K. Laemmli, Cleavage of structural proteins during the assembly of the head of bacteriophage T4, Nature 227 (1970) 680–685.
[23] N. Sreerama, R.W. Woody, Computation and analysis of protein circular dichroism spectra, Methods Enzymol. 383 (2004) 318–351.
[24] T.E. Messick, N.H. Chmiel, M.P. Golinelli, M.R. Langer, L. Joshua-Tor, S.S. David, Noncysteinyl coordination to the $[4Fe–4S]^{2+}$ cluster of the DNA repair adenine glycosylase MutY introduced via site-directed mutagenesis. Structural characterization of an unusual histidinyl-coordinated cluster, Biochemistry 41 (2002) 3931–3942.
[25] S. Lee, G.L. Verdine, Atomic substitution reveals the structural basis for substrate adenine recognition and removal by adenine DNA glycosylase, PNAS 106 (2009) 18497–18502.
[26] H.M. Nash, S.D. Bruner, O.D. Schaerer, T. Kawate, T.A. Addona, E. Spooner, W.S. Lane, G.L. Verdine, Cloning of a yeast 8-oxoguanine DNA glycosylase reveals the existence of a base-excision DNA-repair protein superfamily, Curr. Biol. 6 (1996) 968–980.
[27] M.K. Johnson, Encyclopedia of Inorganic Chemistry, Wiley, New York, 1994.
[28] D.M.H. Ossa, R.R. Oliveira, R.T. Murakami, R. Vincentini, A.J. Costa-Filho, F. Alexandrino, L.M.M. Ottoboni, J.O. Garcia, Expression, purification and spectroscopic analysis of an HdrC: An iron–sulfur cluster-containing protein from *Acidithiobacillus ferrooxidans*, Process Biochem. 46 (2011) 1335–1341.
[29] W.V. Sweeney, J.C. Rabinowitz, Proteins containing 4Fe–4S clusters: an overview, Annu. Rev. Biochem. 49 (1980) 139–161.
[30] D.T. Mapolelo, B. Zhang, S.G. Naik, B.H. Huynh, M.K. Johnson, Spectroscopic and functional characterization of iron–sulfur cluster-bound forms of *Azotobacter vinelandii* ^{Nif}IscA, Biochemistry 51 (2012) 8071–8084.
[31] M.J. Ryle, W.N. Lanzilotta, L.C. Seefeldt, R.C. Scarrow, G.M. Jensen, Circular dichroism and X-ray spectroscopies of *Azotobacter vinelandii* nitrogenase iron protein. MgATP and MgADP induced protein conformational changes affecting the [4Fe–4S] cluster and characterization of a [2Fe–2S] form, J. Biol. Chem. 271 (1996) 1551–1557.
[32] C. Moczygemba, J. Guidry, K.L. Jones, C.M. Gomes, M. Teixeira, P. Wittung-Stafshede, High stability of a ferredoxin from the hyperthermophilic archaeon *A. ambivalens*: involvement of electrostatic interactions and cofactors, Protein Sci. 10 (2001) 1539–1548.
[33] S.S. Leal, C.M. Gomes, On the relative contribution of ionic interactions over iron–sulfur clusters to ferredoxin stability, Biochim. Biophys. Acta 1784 (2008) 1596–1600.
[34] F.F. Xu, J.A. Imlay, Silver (I), mercury (II), cadmium (II), and zinc (II) target exposed enzymic iron–sulfur clusters when they toxify *Escherichia coli*, Appl. Environ. Microbiol. 78 (2012) 3614–3621.
[35] D.H. Nies, Efflux-mediated heavy metal resistance in prokaryotes, FEMS Microbiol. Rev. 27 (2003) 313–339.
[36] D.K. Eggers, J.S. Valentine, Crowding and hydration effects on protein conformation: a study with sol–gel encapsulated proteins, J. Mol. Biol. 314 (2001) 911–922.
[37] E.M. Bowers, L.O. Ragland, L.D. Byers, Salt effects on β-glucosidase: pH-profile narrowing, BBA Proteins Proteom. 1774 (2007) 1500–1507.
[38] D. Constantinescu, H. Weingärtner, C. Herrmann, Protein denaturation by ionic liquids and the Hofmeister series: a case study of aqueous solutions of ribonuclease A, Angew. Chem. Int. Ed. 46 (2007) 8887–8889.
[39] C.L. Higgins, J. Meyer, P. Wittung-Stafshede, Exceptional stability of a [2Fe–2S] ferredoxin from hyperthermophilic bacterium *Aquifex aeolicus*, Biochim. Biophys. Acta 1599 (2002) 82–89.
[40] B.C. Resende, A.B. Rebelato, V. D'Afonseca, A.R. Santos, T. Stutzman, V.A. Azevedo, L.L. Santos, A. Miyoshi, D.O. Lopes, DNA repair in *Corynebacterium* model, Gene 482 (2011) 1–7.